Article

Magnetic Printing of a Biosensor: Inexpensive Rapid Sensing to Detect Picomolar Amounts of Antigen with Antibody-Functionalized Carbon Nanotubes

Abdel Rahman Abdel Fattah, Ahmed M. Abdalla, Sarah Mishriki, Elvira Meleca, Fei Geng, Suvojit Ghosh, and Ishwar K. Puri

ACS Appl. Mater. Interfaces, **Just Accepted Manuscript** • DOI: 10.1021/acsami.6b15989 • Publication Date (Web): 20 Mar 2017

Magnetic Printing of a Biosensor: Inexpensive Rapid Sensing to Detect Picomolar Amounts of Antigen with Antibody-Functionalized Carbon Nanotubes

*Abdel Rahman Abdel Fattah[†,1], Ahmed M. Abdalla[†,2], Sarah Mishriki[†,3], Elvira Meleca[1], Fei Geng[1], Suvojit Ghosh[2] and Ishwar K. Puri[*1,2,3]*

[†] AA, AMA and SM have contributed equally to the work

[1]Department of Mechanical Engineering, [2]Department of Engineering Physics, [3]School of Biomedical Engineering, McMaster University, 1280 Main Street West, Hamilton, Ontario L8S 4L7, Canada

Abstract

When an antibody (Ab) is immobilized on its surface, a carbon nanotube (CNT) becomes a biosensor that detects the corresponding antigen (Ag) since Ag–Ab complexes formed on the CNT surface moderate the current flow through it. We synthesize a biological ink containing CNTs that are twice functionalized, first with magnetic nanoparticles (MNPs) and thereafter with the anti-c-Myc monoclonal Ab. The ink is pipetted and dynamically self organized by an external magnetic field into a dense electrically conducting sensor strip that measures the decrease in current when a sample containing c-Myc Ag is deposited on it. Prototypes are rapidly fabricated materials that cost less than 20 cents (Canadian) for each sensor. With larger current decreases due to real-time specific Ag-Ab binding for higher c-Myc concentrations, the biosensor distinguishes between picomolar c-Myc concentrations within a minute, offering proof of concept of a simple, rapid, economical and sensitive method to detect specific molecules recognizable by Abs.

Keywords: biosensors, magnetic carbon nanotubes, self-assembly, bioinks, antigens

---

*Corresponding Author | **email** ikpuri@mcmaster.ca | **Telephone** 905-525-9140

1. Introduction

The need for early pathogen detection and diagnosis of disease has led to strategies for DNA and antigen (Ag) detection such as polymerase chain reaction (PCR) and enzyme-linked immunosorbent assay (ELISA). Being time consuming and labor intensive, these methods are not suitable for inexpensive rapid detection.[1] Recent advances in nanomaterial synthesis and nanofabrication have enabled the rapid identification of pathogen and disease biomarkers. Nanoscale lithography allows for femtosensitive DNA detection[2-3] and the electrical response of carbon nanotubes (CNTs)[4] to specific biological species has led to resistance and field effect transistor (FET) biosensors.[5-9]

Biosensors can be tailored towards specific biomarkers by selectively modifying a CNT surface, e.g., by decorating it with particular antibodies (Abs), which enables the detection of specific Ags, leading to an inexpensive and rapid alternative to current methods.[10] Usually, fabrication utilizes laborious lithography for electrode deposition and general sensor assembly, while simpler benchtop fabrication methods, e.g., CNTs in paper-based biosensors, provide longer sensing response times.[11]

Magnetic nanoparticles (MNPs) can be patterned into a polymer matrix to produce a functional material.[12-23] MNPs can also be used to guide the deposition of CNTs by remotely manipulating MNP-CNT complexes with a magnetic field, for instance, to print conductive networks and sensors.[12, 24] Magnetic CNTs (mCNTs or CNT-Fe_3O_4 hybrid nanoparticles)) have been explored for biological applications, e.g., human IgG immunosensors,[13] and for electrical current measurements.[9, 25] Most such measurements involve cyclic voltammogram analysis, which requires sophisticated acquisition devices and a magnet to be continually present during sensing to affix the sensing material to an electrode.[26]

Our contribution is through development of a new mCNT biosensor ink that utilizes immobilized Abs to detect specific Ags, which expands the utility of mCNTs as protein-sensing nanomaterials. Without requiring complex chemistry or lithographic techniques, synthesis of the magnetic ink is inexpensive and a sensor strip is readily fabricated. The ink is printed using an external magnet by dynamically self organizing its nanoparticle constituent into an electrically conducting strip in 4-5 minutes, excluding drying time. The resulting biosensor detects Ag samples with picomolar sensitivity in less than a minute.

Biomarkers distinguish between healthy and diseased cells. Examples include prostate-specific antigen (PSA),[27] insulin-like growth factors (IGFs),[28] and human epidermal growth factor receptor (HER)-2,[29] which are used to diagnose human cancers. Recognized by the anti-c-Myc primary Ab, the c-Myc Ag is over-expressed in many human cancers, such as breast, prostate, gastrointestinal, lymphoma, melanoma and myeloid leukemia.[30-31] High expression of c-Myc Ag can accelerate tumour progression,[32] making it a potentially important cancer biomarker for predicting clinical outcomes. Therefore, we focus on c-Myc Ag detection to illustrate proof of concept of an Ab magnetic ink for an Ag sensing application.

The fabrication method is straightforward. (1) First we activate the outer surfaces of CNTs with carboxylic acid function groups by treating them with acid, (2) then tether MNPs, to these surfaces with covalent bonds,[12-22, 33-34] (3) thereafter functionalize the mCNTs with anti-c-Myc Abs,[5, 26] (4) disperse the double functionalized CNTs in DI water, and (5) finally introduce a blocking agent that prevents non-specific protein interactions with the CNT surface through adsorption, increasing detection accuracy. For material characterization, superconducting quantum interference device (SQUID) magnetometry readings are conducted along with X-Ray diffraction (XRD) and transmission electron microscopy

(TEM). Florescence optical microscopy and transmission electron microscopy are used to confirm anti-c-Myc immobilization to the mCNT surfaces.

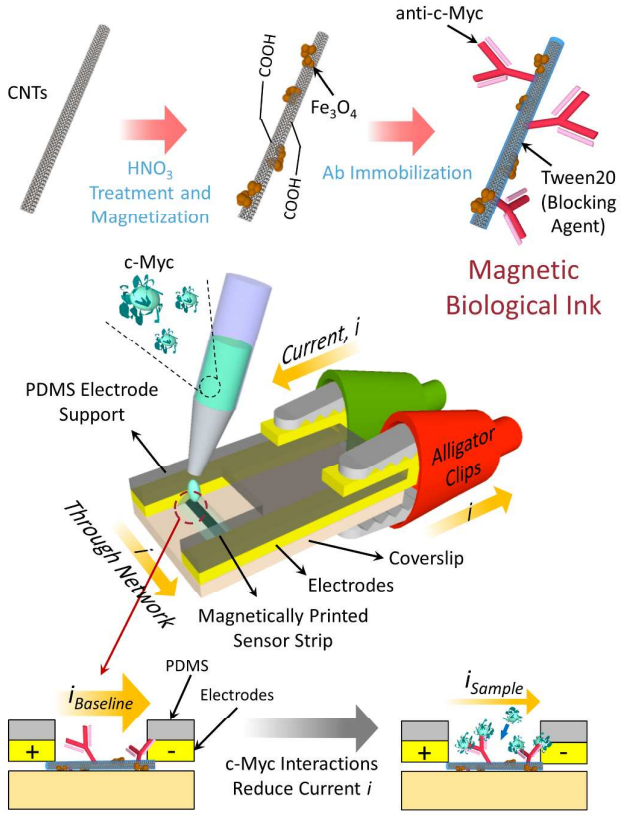

Figure 1. c-Myc Biosensor printing using a magnetic biological ink. Multiwalled CNTs are treated with concentrated nitric acid, which produces carboxylic (–COOH) active groups on the outer surfaces of the CNT. Some of these active groups act as nucleation sites for *in situ* co-precipitation of magnetite (Fe_3O_4) nanocrystals while the remainder remain available for forming covalent bonds with anti-c-Myc amine ($–NH_2$) groups. The CNT surfaces are blocked using Tween 20 to prevent non-specific interactions of Ag with the CNT surface. The magnetic biological ink is then deposited on a glass substrate using a pipette where it self organizes under the influence of an external magnetic field that guides the ink to print a dense electrically conducting strip. After the ink dispersant evaporates, the sensor strip is connected to an external circuit using electrodes. When an aqueous c-Myc solution is deposited on this strip, its electrical resistance increases. A programmable logic controller measures the current flowing through this patterned strip.

2. Results and Discussions

A magnetic field is employed to print the magnetic ink into electrically conducting sensing strips, which are integrated into an external circuit using simple electrodes. Placing a sample containing c-Myc Ags on a sensing strip initiates specific Ag-Ab interactions, reducing the electric current passing through the strip. The current reduction, which is the c-Myc detection signal, is measured using a programmable logic controller (PLC), see **Figure 1**.

Sensor fabrication is inexpensive, signal detection is rapid, and our benchtop fabrication method is scalable since the ink can be readily integrated into standard inkjet and 3D printers. The small ink volumes required for sensor fabrication and the magnet-independent electrical measurements make the ink attractive for integration into drug screening and disease detection applications.

2.1. Magnetized Carbon Nanotubes. The first step during ink production requires that CNTs be treated with concentrated HNO_3, which creates surface sites where reactive molecules, such as COOH, C=O, and C–OH, form covalent bonds with the CNT scaffold and where magnetite nanocrystals (Fe_3O_4) are subsequently nucleated.[33] The material characterization of the magnetized multiwalled CNTs is shown in **Figure 2**. XRD, TEM and SQUID measurements confirm that the CNTs are successfully decorated with crystalline Fe_3O_4 magnetic nanoparticles.

XRD analysis of dried mCNTs is conducted for Fe_3O_4:CNT at three weight ratios $\gamma = 0.1$, 0.2, and 0.4. **Figure 2**(a) shows that all samples consist only of the intended magnetite and carbon phases. The powder diffraction file (PDF) database, available through the Eva software, qualitatively confirms that all three samples contain hexagonal carbon (carbon nanotubes, PDF No. 00-058-1638) and the spinel magnetite phase (Fe_3O_4, PDF No. 01-071-6336). The average size of the Fe_3O_4 nano-crystals is calculated through the Scherrer equation applied at the highest diffraction peak (311).

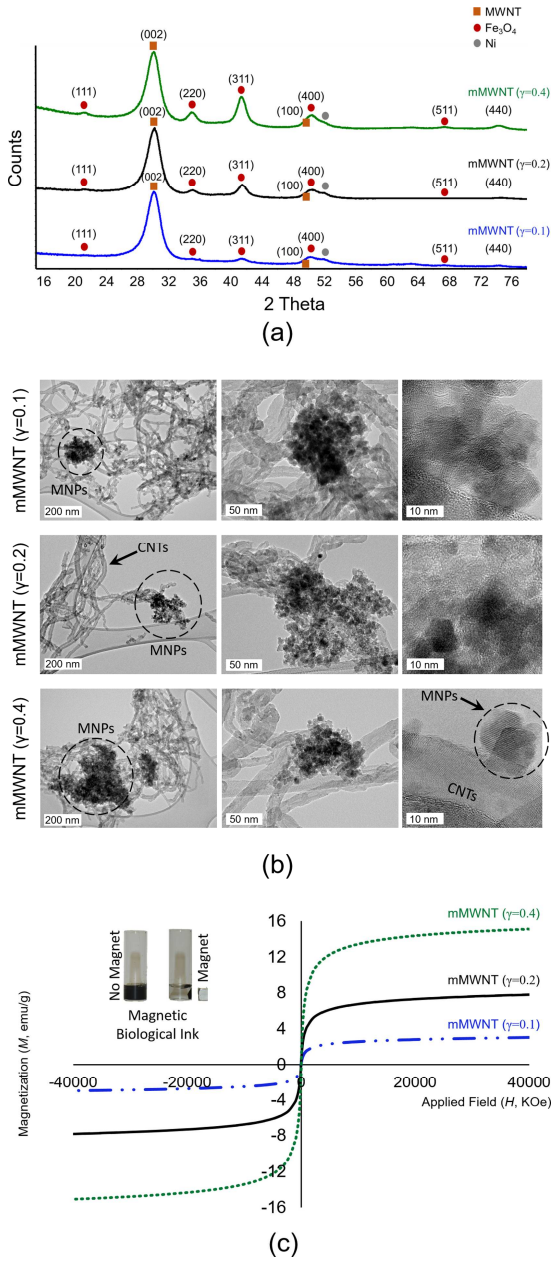

Figure 2. Characterization of Magnetized Multi-Walled Carbon Nanotubes. (a) **X-Ray Diffraction Analysis of mCNTs.** The XRD (Co K_α, λ=1.79 Å) patterns for magnetite to CNTs weight ratios γ = 0.1, 0.2, and 0.4 confirm the presence of a magnetite (Fe_3O_4) phase and a hexagonal carbon phase that originates from the carbon nanotubes. (b) TEM images of magnetized multiwall CNT samples at various magnetization weight ratios γ = 0.1 to 0.4 (from top to bottom) confirm that all samples have been successfully decorated with highly crystalline MNPs that are synthesized within a narrow size distribution around ~10 nm. (c) **Magnetic Characterization.** Magnetic hysteresis curves show that all magnetized CNT samples exhibit superparamagnetic behaviour, but have different saturation values M_s depending on γ. The greater the magnetite content, the stronger is the material response to a magnetic field.

For all three samples, the MNP sizes lie in a narrow 8.6–10.3 nm range. Using Bragg's Law, calculations of the average lattice parameters of Fe_3O_4 are 8.403, 8.396 and 8.404 Å for γ = 0.1, 0.2, and 0.4. These values agree with those for magnetite (8.394 Å, JCPDS No. 79-0417; and 8.400 Å, COD card No. 1011084). The TEM micrographs in **Figure 2**(b) show that the CNT surfaces are decorated with highly crystalline MNPs that have a narrow crystallite size distribution around ~10 nm. Increasing γ improves the decoration density.

Because of their small sizes, the magnetite nanoparticles are superparamagnetic [35] with a high saturation magnetization. Conjugating the MNPs with the diamagnetic CNTs retains this superparamagnetic behavior, which is evident in **Figure 2**(c) since the measured hysteresis loops for all of the cases indicate that there is no remanence or coercive field. The magnetic saturations M_s = 3.03, 7.79, 15.09 emu/g for γ = 0.1, 0.2 and 0.4. A higher M_s value translates into a stronger magnetic response for the conjugate material, which assists magnetic printing, producing a denser and more electrically continuous biosensor strip. Being superparamagnetic, dipole-dipole interactions in the conjugate material are limited in the absence of a magnetic field, for instance during storage, which reduces nanoparticle aggregation, allowing repeatable sensor printing.

2.2 Antibody Immobilization. Next, the CNT surfaces are functionalized with anti-c-Myc Abs through two pathways. The relatively low MNP yield allows some active carboxylic groups to remain post magnetization. Hence, subsequent addition of anti-c-Myc allows the Ab to become covalently bonded even without intermediate reagents[26] through a condensation reaction between the Ab amine groups and the remaining carboxylic groups on the mCNT surfaces.[5-6, 8, 36-38] Alternately, Abs can also be physically adsorbed on this surface but, as we explain later, in this case Ab-Ag binding kinetics cannot be determined using the biosensor. Here, since the CNTs are not treated with acid, their surface defect sites lack carboxylic acid groups. Thus instead of forming covalent bonds, Abs are simply adsorbed on to the CNT surfaces. The

absence of carboxylic acid groups also prevents the covalent attachment of MNPs, which are now also only adsorbed though a simple sonication step with the CNTs. The final ink preparation step involves dispersing the mCNT-Ab hybrid nanoparticles in an aqueous solution of Tween 20 (polysorbate 20), which acts as a blocking agent, coats the CNT surface, and prevents non-specific Ag-Ab binding.

The binding of Ab molecules to CNTs is visualized through fluorescent microscopy. Secondary Ab, fluorescein isothiocyanate (FITC)-conjugated Donkey anti-Mouse IgG H&L, is used to create a fluorescent ink, for which the Ab:CNT weight ratio $\beta = 2.5\times10^{-4}$. The fluorescence intensity is invariant to the Fe_3O_4:CNT weight ratio γ in the range 0.1-0.4, as shown **Figure 3**(a)–(c), i.e., the magnetization of CNTs has a negligible impact on Ab immobilization on the nanotube surfaces. Hence, CNTs magnetized with $\gamma = 0.4$, which exhibit robust magnetic response, are used to fabricate the biosensor strip.

The fluorescence images for CNT samples with covalently bonded Abs in **Figure 3**(a)–(c) are virtually indistinguishable from the image in **Figure 3**(d), which reveals Abs that are adsorbed onto as-manufactured nanotube surfaces that do not contain functional groups. Thus, for the particular Ab:CNT weight ratio used, there appears to be no difference in Ab immobilization on nanotube surfaces corresponding to (1) mCNTs, or (2) as manufactured CNTs that have no surface functional groups at acid-induced defect sites. There is no fluorescence in the absence of Ab conjugation, i.e., when $\beta = 0$, see **Figure 3**(e), confirming that the fluorescence sources in **Figure 3**(a)-(d) are due to FITC-labeled Abs only.

Since anti-c-Myc Ab is non-fluorescent, an electron energy loss spectrum (EELS) is performed to identify Abs on the mCNT surfaces. **Figure 3**(f) depicts a scanning transmission electron microscopy (STEM) micrograph and the corresponding EELS spectrum for the ink. The spectrum highlights locations where elemental C, O and N are present. Since

N originates solely from the Abs and no other ink component, its map reveals anti-c-Myc locations. The micrograph uncovers a general structure that consists of a CNT-Fe_3O_4-Ab network, where the CNT mesh produces the electrical path and the Abs are Ag receptor sites.

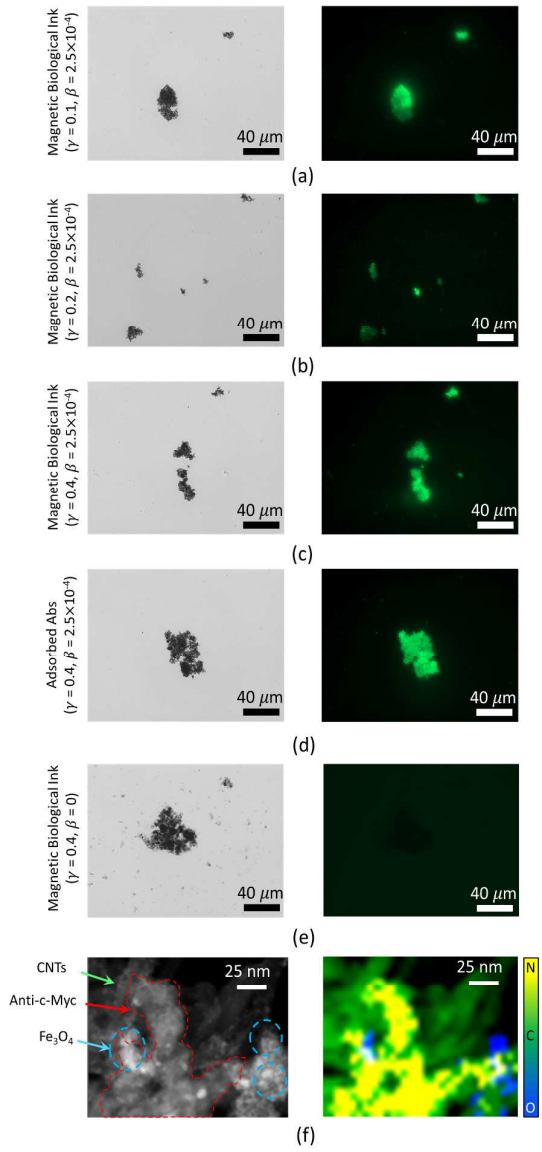

Figure 3. Visualization of Ab immobilization on the surface of magnetic CNTs. First, FITC-labeled fluorescent Abs are employed to confirm Ab immobilization on the surface of magnetic CNTs for an Ab:CNT weight ratio $\beta = 2.5\times10\text{-}4$ in an ink where Abs are covalently bonded with magnetized CNTs that have Fe_3O_4:CNT weight ratios (a) $\gamma = 0.1$, (b) $\gamma = 0.2$ and (c) $\gamma = 0.4$, and (d) for an ink that contains Abs and MNPs, which are instead simply adsorbed on the surface of CNTs with $\gamma = 0.4$. For (e) $\beta = 0$, $\gamma = 0.4$, no fluorescence is observed from CNTs and Fe_3O_4, confirming that the fluorescence observed in (a)-(d) originates from FITC-labeled Abs only. No visual differences in fluorescence are detected for samples containing different weight ratios of magnetite, and those containing adsorbed and covalently bonded immobilized Abs and MNPs. For (a)-(e), the images on the left column are optical bright field and the images on the right column are bright field and

fluorescent overlay. (f) STEM and EELS micrographs reveal the presence of elemental carbon (C), oxygen (O) and nitrogen (N). The nitrogen, which is present only in Anti-c-Myc Abs, confirms Ab immobilization on the conductive CNT network.

2.3. Fabrication of the Bio-sensor. The device is fabricated as shown in **Figure 4**(a). A 10 μL volume of the magnetic biological ink is deposited with a micropipette over a 7 mm length on a glass coverslip directly above one of the magnet edges, which concentrates the magnetic field locally, which dynamically self organizes the magnetized and Ab-functionalized CNTs into a dense electrically conducting strip. After it is printed, each sensor is dried for 20 minutes at room temperature in the presence of the magnetic field, which maintains the integrity of the mCNT-Ab conjugate. When the dispersing medium (DI Water) has evaporated, dried printed sensor strips of ~7 mm length and ~1.5 mm width remain on the coverslip, held in place by Van der Waals and electrostatic forces. Despite visual observations of cracks, strips at different times exhibit identical sensing responses to various samples.

Typically, each sensor consists of ~100 μg of CNTs, ~40 μg of Fe_3O_4 and ~25 ng of anti-c-Myc Ab, i.e., the material usage per sensor is small. Hence, the material cost of a printed sensor is lower than 20 cents (Canadian). The sensor is integrated with electrodes using a polydimethylsiloxane (PDMS) support and alligator clips that connect the strip to an electrical circuit. With a reference resistance R_{ref}, an external circuit is used to measure real-time current changes when samples are deposited on the biosensor, see **Figure 4**(b).

2.4 Sensing Measurements. Two types of tests are performed. (1) A sample is deposited once on the surface of the printed biosensor strip, and (2) equal amounts of the sample are deposited repeatedly after specific intervals on the sensor surface. Three tests are performed with every sample, each with a newly printed biosensor. **Figure 5**(a) presents temporal responses when 2 μL of (1) purified c-Myc with 40, 20, and 10 pM concentrations, (2) DI

water, and (3) 40 pM concentration of bovine serum albumin (BSA) are placed on the biosensor. The BSA is a nonspecific Ag towards anti-c-Myc Ab and is therefore a negative control.

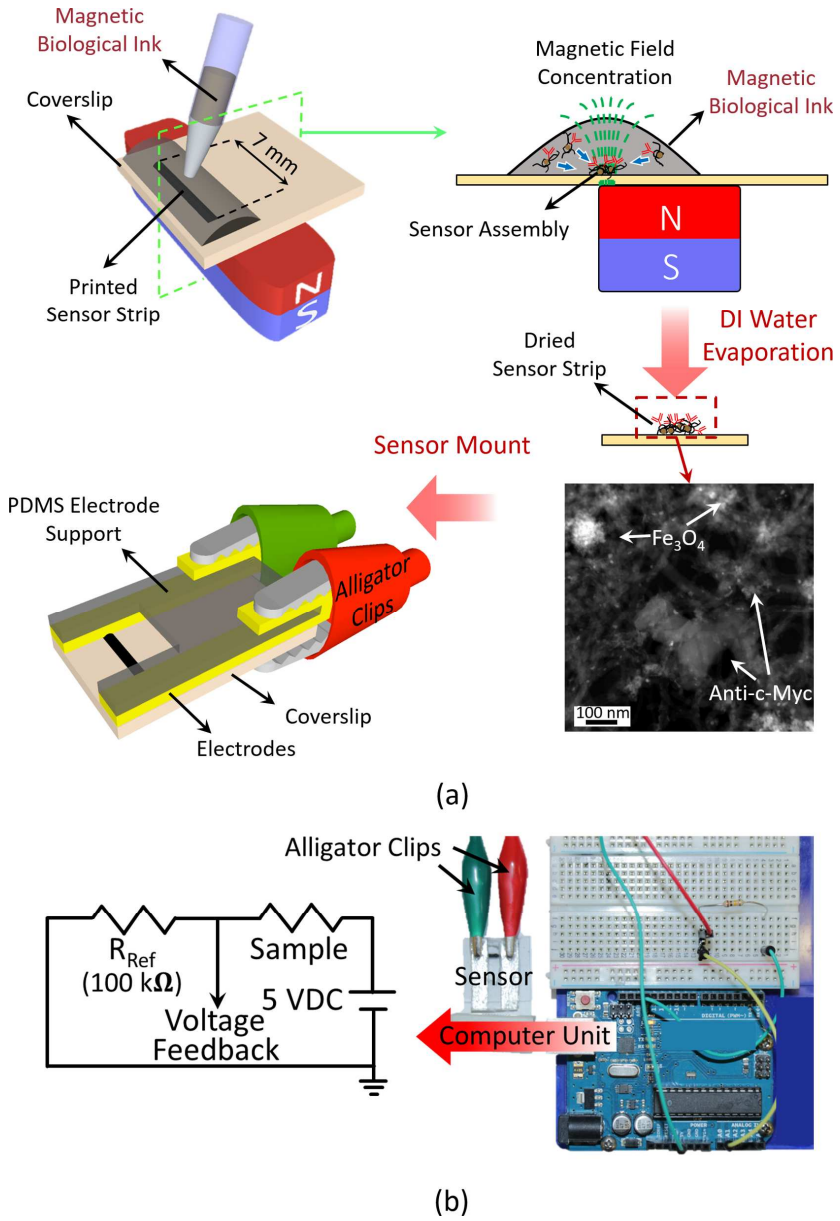

Figure 4. Printing technique and sensor assembly. (a) 10 µL of the magnetic bioink is deposited on top of a glass coverslip that is placed on a permanent magnet. The applied magnetic field concentrates and self organizes the functionalized magnetic CNTs on the substrate. After the supernatant in the ink is evaporated, a patterned strip of densely packed Ab-functionalized CNTs remains deposited on the substrate, which forms the sensor. The STEM micrograph identifies MNPs and anti-c-Myc that constitute the print based on the magnetic bioink. Electrodes are readily connected to either end of the strip, providing current to the sensor. (b) A voltage divider with a reference resistor R_{ref} = 100 kΩ monitors current changes that measure the biosensor responses to the various samples that are deposited on it.

Figure 5(a) shows that after sample deposition at time t = 2s on an initially dry biosensor, the current i_s decreases rapidly from its initial value $i_b \approx 47$ μA before reaching steady state. Both DI water and BSA samples induce similar decreases in the biosensor current. In contrast, i_s does not level off as quickly when c-Myc is deposited on the strip, but continues to decrease below the steady values reached for DI water and BSA. The biosensor responds differently to c-Myc sample deposition due to the specific interaction of anti-c-Myc Ab with the c-Myc Ag. This increases the electrical resistance of the sensor, which in turn decreases i_s.[39-40] Nonspecific interactions of anti-c-Myc with DI water and BSA do not decrease i_s as significantly below its initial value. The relatively slow Ag-Ab binding induce the gradual current reduction.

The biosensor responses shown in **Figure 5**(a) underscore the specificity with which the ink detects c-Myc. Increasing the Ag concentration enhances Ab binding and thus, the electrical resistance of the sensor strip, which leads to a larger current reduction and steeper temporal current gradients di_s/dt, as shown in **Figure 5**(a). The values of i_s at t = 60 s for the 40, 20, and 10 pM c-Myc concentrations are 34.6±0.5, 38.8±0.4, and 40.9±0.1 μA, respectively, confirming that current reduction scales with increasing Ab concentration.

During $30 < t < 60$ s, the gradient di_s/dt is constant, which also correlates with the c-Myc concentration. **Figure 5**(b) presents the ratio $i_{s,a}/i_{s,a,30s}$, where $i_{s,a}$ is the temporal current at time t averaged over three repetitive tests for a sample and $i_{s,a,30s} = i_{s,a}$ at t = 30 s. **Figure 5**(c) reveals linear correlations between the current gradients obtained from **Figure 5**(b) and the c-Myc concentrations. Both **Figure 5**(b) and **Figure 5**(c) are the result of 12 identically printed devices, i.e. 3 for each case of 10 pM, 20 pM, and 40 pM of c-Myc and 40 pM of BSA. These correlations are in agreement with reported responses for CNT-based biosensors.[5, 25-26] By simply monitoring the sensor's transient electrical response, it is possible to rapidly identify

c-Myc positive samples with different concentrations. This makes Ag monitoring feasible without using additional reagents and sophisticated electrical equipment that is typical of other biosensors.[26]

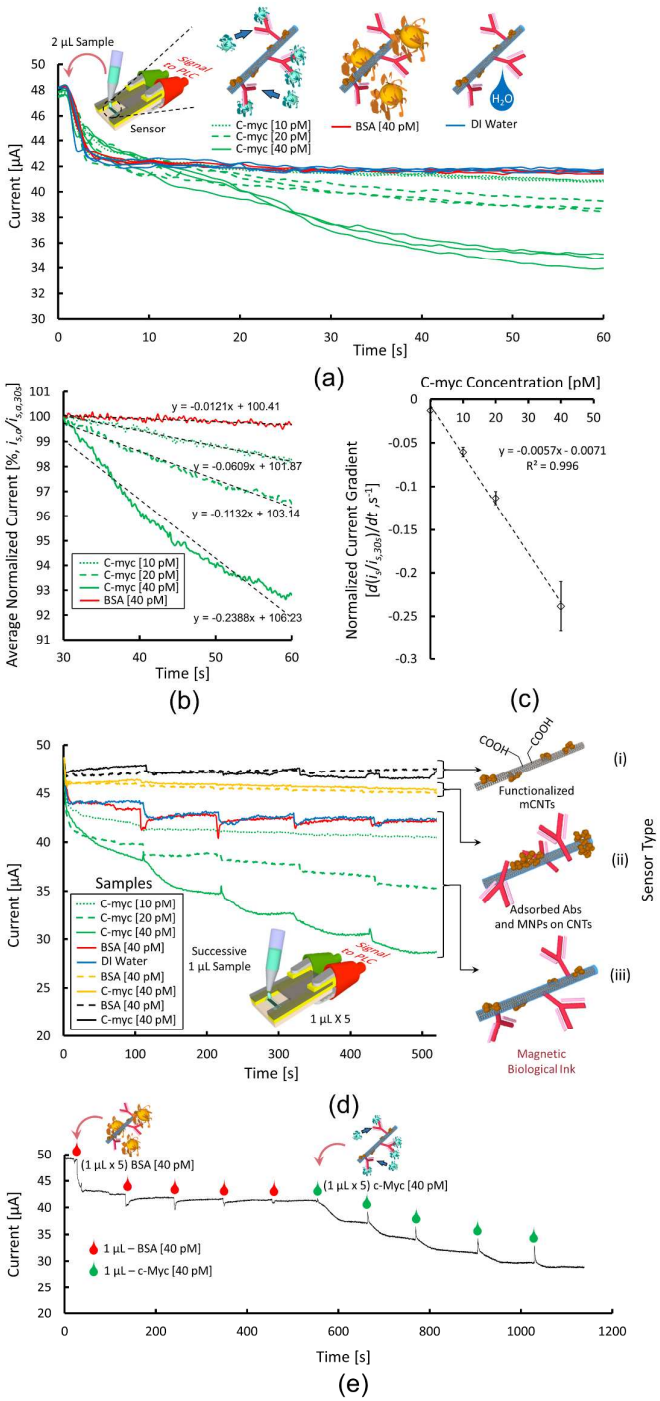

Figure 5. Biosensor transient response. (a) Immediately after 2 µL samples are deposited on the sensor strip, the DI water and BSA samples induce a rapid decrease in electrical current, which

subsequently levels out. In contrast, since the sensor is inherently sensitive to c-Myc Ag interactions due to the anti-c-Myc Abs that are covalently bonded to the surfaces of CNTs, the current for all c-Myc samples decreases to levels below those measured for DI water and BSA deposition, which offers proof of targeted detection and sensor specificity to c-Myc Ags. The higher the c-Myc concentration in a sample, the larger the current decrease it induces. All of the deposited c-Myc samples produce a steady current decrease during the period 30 s < t < 60 s. Normalizing the average current over that duration leads to the quasi-linear response shown in (b). There is a linear correlation in (c) between the normalized current gradients in (b) and the corresponding c-Myc concentrations. **Biosensor response to successive 1 µL sample additions.** (d) Acting as a control, magnetized CNTs that are not functionalized with Abs (i) cannot distinguish between 40 pM BSA and c-Myc samples, black dashed and solid curves respectively. When anti-c-Myc is immobilized on the CNT surfaces through adsorption, again (ii) there is insufficient discrimination between these two samples. In contrast, a sensor fabricated using an ink in which anti-cMyc is attached to the CNT surfaces through acid functionalization, (iii) clearly distinguishes between the two negative control samples, DI water and BSA, and the Ag of interest, c-Myc. (e) After the deposition of 5 successive 1 µL samples of BSA [40 pM], the biosensor response is relatively unchanged. Only after the introduction of c-Myc [40 pM] samples that the reduction in current is observed, validating the specificity of the sensor to the target antigen in the presence of another protein.

Defect sites on CNT surfaces restrict electron transport, since they increase the resistance[37-38] to the passage of electrical current. Following acid treatment of the CNTs, these sites become populated with active carboxylic acid groups that are capable of hosting Abs. Each carboxylic group is capable of forming a covalent bond with the amine group of an Ab through a condensation reaction. When the target Ag binds to its corresponding Ab, the circuit experiences additional electrical resistance. Through their interactions with defect sites, covalent Ab immobilization amplifies the resistance over the effect produced by an Ab that is simply adsorbed. In the former case, an Ag binding to an Ab provides an additional interaction with a defect site to increase the overall resistance.

The response of the biosensor to successive 1 µL sample depositions is presented in **Figure 5**(d) for three types of biosensor strips that are printed with three different inks. These inks contain (i) covalently magnetized CNTs that have not yet been functionalized with Abs (ink 1), or (ii) CNTs that have both Fe_3O_4 nanoparticles and anti-c-Myc Abs adsorbed on their surfaces (ink 2), and (iii) CNTs that are covalently magnetized with Fe_3O_4 nanoparticles and contain both covalently bonded and adsorbed anti-c-Myc Abs on their surfaces (ink 3).

The functionalized CNTs for all three inks are dispersed in DI water containing 0.1% Tween 20.

Biosensors printed with inks 1 and 2 do not discriminate between 40 pM c-Myc Ag and 40 pM BSA, i.e., they produce similar responses for these two samples and it is not possible to positively detect c-Myc by printing biosensor strips with these two inks. The biosensor remains specific to the target antigen in the presence of another protein molecule. Figure 5(e) shows the relatively unchanged signal with the addition of 5 successive 1 uL of BSA [40 pM]. When c-Myc [40 pM] samples are subsequently deposited on the sensor, a reduction in current is observed, signifying a positive detection. This reduction in current is similar to that observed in Figure 5(d) for the same c-Myc concentration. Additional experiments are required to show stable specificity in the presence of multiple non-specific proteins. This can be done by controlling the expression of c-Myc in a cell line versus a control, and using whole cell lysate to perform the tests.

4. Conclusions

Biological ink containing Abs immobilized on the surfaces of magnetized CNTs that are dispersed in DI water containing a bio-compatible surfactant, Tween 20, is synthesized. Ink synthesis is straightforward and does not involve complex chemistry or use of intermediate reagents. An applied magnetic field dynamically self organizes the magnetized and functionalized CNTs, printing them into an electrically responsive strip that serves as a biosensor to detect specific Ags. Unlike previous methods, a magnet is not required during sensing, facilitating simple integration of the sensor into an electric circuit. The sensor detects picomolar c-Myc concentrations within a minute and distinguishes between c-Myc and BSA samples of different concentrations through decreases in the sensor current. These decreases, which occur due to real-time specific Ab-Ag binding, are larger at higher Ag concentrations.

The detection technique is simpler, inexpensive and rapid as compared to typical cyclic voltammorgam analysis. Once the ink is synthesized, the time required to create a prototype sensor is less than 5 minutes, excluding ink drying time. Semi-quantitative Ag detection with picomolar sensitivity occurs within a minute after a sample is deposited on the biosensor. This proof of concept ink and sensor can be tailored to detect different Ags.

5. Experimental Section

Materials and Reagents. Multiwall CNTs produced by CVD with purity > 95%, outside diameters of 20-30 nm, inside diameters of 5-10 nm and lengths between 0.5-2.0 μm were purchased from US Research Nanomaterials. Other reagents used included ferric chloride hexahydrate ($FeCl_3 \cdot 6H_2O$, 97-102%, Alfa Aesar), ferrous chloride tetrahydrate ($FeCl_2 \cdot 4H_2O$, 98%, Alfa Aesar), nitric acid (HNO_3, 68-70%, CALEDON), and ammonium hydroxide (NH_4OH, 28-30%, CALEDON). C-Myc Ag (Abcam, Cambridge, Massachusetts, USA) had a molecular weight of 49 kDa (49,000 g mol^{-1}). Bovine serum albumin (BSA) (Sigma Aldrich, Oakville, Ontario, Canada) was used as a negative control. All reagents were used as received without further purification. The NdFeB, Grade N52 magnets were purchased from K&J Magnetics Inc (25.4×6×6 mm). The electrode support was fabricated using polydimethylsiloxane (PDMS) and a curing agent (Sylgard 184 kit, Dow Corning). The coverslips (Fisher Scientific, 12-540-B) had dimensions of 22×22×2 mm.

Characterization Methods and Instruments. XRD analysis of CNT and mCNT powder samples was performed using a Bruker D8 Discover instrument comprising a DavinciTM diffractometer operating at 35 kV and 45 mA using Co-Kα radiation (λ_{avg} = 1.79026 Å). Bruker's DIFFRAC.Eva V3.1 and TOPAS software were used for the analysis and semi-quantitative estimation of the sample composition. TEM and EELS spectroscopy were conducted with a JEOL 2010F field emission microscope, where the samples were suspended

in ethanol, dripped on to a TEM grid and then wicked off with a tissue-wipe. Optical and fluorescence (Enhanced Green Fluorescent Protein, EGFP) microscopy were conducted using a Zeiss Axio Observer.Z1. Magnetization measurements were performed using a SQUID magnetometer at room temperature.

Production, purification and quantification of anti-c-Myc monoclonal Abs. 9e10 hybridoma cells were used to produce anti-c-Myc Abs that were then purified with a centrifugal filter to remove fetal bovine serum (FBS) from the cell culture media (Amicon® Ultra-4 Centrifugal Filter with 3k molecular weight limit, and Amicon® Ultra-15 Centrifugal Filter with 100k molecular weight limit). The purified anti-c-Myc Abs were analyzed with SDS-PAGE and their quantification was performed with a Qubit 2.0 Fluorometer. Concentration of the anti-c-Myc Ab suspension resulted in a 0.5 mg/mL concentration.

Two-step Functionalization of Carbon Nanotubes: Magnetite and anti-cMyc. The CNTs were functionalized in the manner we have previously reported. [33] Briefly, 1 g of CNTs was activated by dispersing it in 200 mL of concentrated nitric acid. The suspension was sonicated for 4 h in a sonication bath (VWR International, Model: 97043-936). The activated CNTs (aCNTs) were subsequently washed several times with deionized (DI) water, filtered, washed again and finally dried in a vacuum oven. Magnetite nanoparticles were co-precipitated onto the aCNTs by stoichiometric calculations to obtain a Fe_3O_4:aCNTs magnetization weight ratios $\gamma = 0.1$, 0.2, and 0.4 (w/w). For $\gamma = 0.4$, a 0.92 g $FeCl_3 \cdot 6H_2O$ and 0.36 g $FeCl_2 \cdot 4H_2O$ mixture was dissolved in 160 mL of degassed DI water. This was followed by ultrasonic dispersion of 1 g of the aCNTs for 10 mins with a probe sonicator (Qsonica, Model: Q500 with 1/4″ micro-tip at 35% power) and subsequently for 50 minutes in a sonication bath at 50° C. A 2 ml 30% ammonia solution was slowly introduced as a precipitant to increase the pH to 9. The magnetized CNTs thus produced were washed several times until pH ~ 7 was reached, and then filtered and dried in a vacuum oven for 1 hr. In the

case of adsorbed MNPs on the surface of CNTs, a previous methodology [12] allowed us to entangle magnetite and CNTs, yielding $\gamma = 0.4$.

Immobilization of anti-c-Myc Abs on mCNTs. Following activation and magnetization of the CNTs, Ab immobilization was performed. For each mg of CNTs contained in the magnetized CNTs, 2 mL of deionized water was used as media to disperse the precursor magnetic ink in solution with a probe sonicator (15 seconds, 30% amplitude). An anti-c-Myc to CNT weight ratio $\beta = 2.5\times10^{-4}$ value was selected and an appropriate amount of Ab (0.5 µL, 0.5 mg mL^{-1}) was added to the magnetized CNTs (1.4 mg) in solution. The mixture was incubated for 1 hour at room temperature, inverted gently every five minutes to maintain the suspension, or when sedimentation of the magnetic biological ink was observed. Following incubation, the supernatant was removed.

A blocking procedure was performed to prevent non-specific binding of Ag molecules to the ink. Blocking of the CNT surface ensures that the detected signal is directly related to the specific Ag-Ab interaction, reducing noise that may originate due to adsorption of non-specific molecules. [5, 41] For every 1 mg of activated CNTs, 2 mL of blocking solution (0.1% Tween 20 in deionized water) was added to the magnetic biological ink. [8] The ink was blocked for a half hour at room temperature, inverted gently every five minutes to ensure saturation of the nanoparticle surfaces in the ink. Following incubation with the blocking solution, the ink was washed three times in deionized water. A final concentration of 10 mg/mL was obtained by adjusting the amount of DI water. The same approach was followed for the case when MNPs and Ab were adsorbed on the CNT surfaces.

Electrical Circuit, Sensor Assembly and Sensing. To investigate the sensing capability of the dried ink, a voltage divider circuit was used with a reference resistance of R_{ref} = 100 kΩ. A square PDMS (2.5×2.5×0.3 cm) section was used to support two aluminum

foil electrodes. The PDMS was fabricated using a mold with a mixture of the PDMS precursor and PDMS curing agent (10:1 w/w), which was subsequently degassed for 20 min and cured at 70˚C in an oven. The electrodes were separated by 5 mm and fixed to the PDMS support using double-sided tape. A cutout (1×0.5 cm) through the PDMS support was centered between the electrodes to allow sample deposition on the ink strip. The electrodes were wrapped around this support to provide electrical access with alligator clips. The PDMS electrode assembly was positioned on the top of the sensor, while the alligator clips held the sensor assembly together mechanically. This ensured good connection between the ink network and the aluminum electrodes. Each electrode covered a ~1 mm section of the sensor, leaving another 5 mm ink strip exposed for sample deposition and therefore Ag detection. The printed sensor of resistance R_s was connected in series with R_{ref}. A PLC (Arduino Uno) supplied the circuit with a 5 V DC power supply, while an analog feedback voltage allowed the PLC and computer unit to interpret and sample the current i passing through the circuit at a frequency of 10 Hz. After each test, the electrodes were wiped with ethanol (100%) and left to dry to ensure that no cross contamination occurred.

Author Information

Corresponding Author

*Tel: 905-525-9140 ext: 24900. E-mail: ikpuri@mcmaster.ca

Author Contributions

The manuscript was written through contributions of all authors. All authors have given approval to the final version of the manuscript.

Notes

The authors declare no competing financial interest.

Acknowledgements

This work is supported by a Natural Sciences and Engineering Research Council of Canada (Grant no. RGPIN-2014-04066) Discovery Grant (NSERC-DG), and Canada Foundation for Innovation John R. Evans Leaders Fund (CFI-JELF) and Ontario Research Fund Research Infrastructure (ORF-RI) grants (Grant no. 33016). For assistance with measurements, we thank Dr. Carmen Andrei of the Canadian Centre for Electron Microscopy (CCEM) for TEM, Dr. Paul Dube of the Brockhouse Institute for Materials Research, McMaster University for SQUID, and Vicky Jarvis of the McMaster Analytical X-Ray Diffraction Facility (MAX) for XRD. The CCEM is a national facility supported by NSERC, Canada Foundation for Innovation and McMaster University.

References

(1) Kolosovas-Machuca, E. S.; Vera-Reveles, G.; Rodriguez-Aranda, M. C.; Ortiz-Dosal, L. C.; Segura-Cardenas, E.; Gonzalez, F. J., Resistance-Based Biosensor of Multi-Walled Carbon Nanotubes. *J. Immunoassay Immunochem.* **2015,** *36*, 142-148.

(2) Soleymani, L.; Fang, Z.; Sun, X.; Yang, H.; Taft, B. J.; Sargent, E. H.; Kelley, S. O., Nanostructuring of Patterned Microelectrodes To Enhance the Sensitivity of Electrochemical Nucleic Acids Detection. *Angew. Chem., Int. Ed.* **2009,** *48*, 8457-8460.

(3) Alubaidy, M.; Soleymani, L.; Venkatakrishnan, K.; Tan, B., Femtosecond Laser Nanostructuring for femtosensitive DNA detection. *Biosens. Bioelectron.* **2012,** *33*, 82-87.

(4) Tiwari, J. N.; Vij, V.; Kemp, K. C.; Kim, K. S., Engineered Carbon-Nanomaterial-Based Electrochemical Sensors for Biomolecules. *ACS Nano.* **2015,** *10*, 46-80.

(5) Balasubramanian, K.; Burghard, M., Biosensors Based on Carbon Nanotubes. *Anal. Bioanal. Chem.* **2006,** *385*, 452-68.

(6) Li, C.; Curreli, M.; Lin, H.; Lei, B; Ishikawa, F. N.; Datar, R; Cote, R. J.; Thompson, M. E.; Zhou, C., Complementary Detection of Prostate-Specific Antigen Using In_2O_3 Nanowires and Carbon Nanotubes. *J. Am. Chem. Soc.* **2005,** *127*, 12484-12485.

(7) Chen, R. J.; Bangsaruntip, S.; Drouvalakis, K. A.; Kam, N. W.; Shim, M.; Li, Y.; Kim, W.; Utz, P. J.; Dai, H., Noncovalent Functionalization of Carbon Nanotubes for Highly Specific Electronic Biosensors. *Proc. Natl. Acad. Sci. U. S. A.* **2003,** *100*, 4984-4989.

(8) Cid, C. C.; Riu, J.; Maroto, A.; Rius, F. X., Carbon Nanotube Field Effect Transistors for the Fast And Selective Detection of Human Immunoglobulin G. *Analyst* **2008,** *133*, 1005-1008.

(9) Liu, Z.; Wang, J.; Xie, D.; Chen, G., Polyaniline-Coated Fe_3O_4 Nanoparticle-Carbon-Nanotube Composite and its Application in Electrochemical Biosensing. *Small* **2008,** *4*, 462-466.

(10) Lerner, M. B.; Pan, D.; Gao, Y.; Locascio, L. E.; Lee, K.-Y.; Nokes, J.; Afsahi, S.; Lerner, J. D.; Walker, A.; Collins, P. G., Large Scale Commercial Fabrication of High Quality Graphene-Based Assays for Biomolecule Detection. *Sens. Actuators, B* **2017,** *239*, 1261-1267.

(11) Pozuelo, M.; Blondeau, P.; Novell, M.; Andrade, F. J.; Xavier Rius, F.; Riu, J., Paper-Based Chemiresistor for Detection of Ultralow Concentrations of Protein. *Biosens. Bioelectron.* **2013,** *49*, 462-465.

(12) Abdel Fattah, A. R.; Majdi, T.; Abdalla, A. M.; Ghosh, S.; Puri, I. K., Nickel Nanoparticles Entangled in Carbon Nanotubes: Novel Ink for Nanotube Printing. *ACS Appl. Mater. Interfaces* **2016,** *8*, 1589-1593.

(13) Masotti, A.; Caporali, A., Preparation of Magnetic Carbon Nanotubes (Mag-CNTs) for Biomedical and Biotechnological Applications. *Int. J. Mol. Sci.* **2013,** *14*, 24619-24642.

(14) Meng, L.; Fu, C.; Lu, Q., Advanced Technology for Functionalization of Carbon Nanotubes. *Prog. Nat. Sci.* **2009,** *19*, 801-810.

(15) Balasubramanian, K.; Burghard, M., Chemically Functionalized Carbon Nanotubes. *Small* **2005,** *1*, 180-92.

(16) Korneva, G.; Ye, H.; Gogotsi, Y.; Halverson, D.; Friedman, G.; Bradley, J. C.; Kornev, K. G., Carbon Nanotubes Loaded with Magnetic Particles. *Nano Lett.* **2005,** *5*, 879-884.

(17) He, H.; Gao, C., Synthesis of Fe_3O_4/Pt Nanoparticles Decorated Carbon Nanotubes and Their Use as Magnetically Recyclable Catalysts. *J. Nanomater.* **2011,** *2011*, 1-10.

(18) Abdel Fattah, A. R.; Ghosh, S.; Puri, I. K., Printing Microstructures in a Polymer Matrix Using a Ferrofluid Droplet. *J. Magn. Magn. Mater.* **2016,** *401*, 1054-1059.

(19) Ganguly, R.; Puri, I. K., Field-Assisted Self-Assembly of Superparamagnetic Nanoparticles for Biomedical, MEMS and BioMEMS Applications. *Adv. Appl. Mech.* **2007,** *41*, 293-335.

(20) Ganguly, R.; Puri, I. K., Microfluidic Transport in Magnetic MEMS and BioMEMS. *Wiley Interdisciplinary Rev.: Nanomed. Nanobiotech.* **2010,** *2*, 382-399.

(21) Puri, I. K.; Ganguly, R., Particle Transport in Therapeutic Magnetic Fields. *Annu. Rev. of Fluid Mech.* **2014,** *46*, 407-440.

(22) Abdel Fattah, A. R.; Ghosh, S.; Puri, I. K., Printing Three-Dimensional Heterogeneities in the Elastic Modulus of an Elastomeric Matrix. *ACS Appl. Mater. Interfaces* **2016,** *8*, 11018-11023.

(23) Tsai, P. J.; Ghosh, S.; Wu, P.; Puri, I. K., Tailoring Material Stiffness by Filler Particle Organization. *ACS Appl. Mater. Interfaces* **2016,** *8*, 27449-27453.

(24) Qu, S.; Wang, J.; Kong, J.; Yang, P.; Chen, G., Magnetic Loading of Carbon Nanotube/Nano-Fe_3O_4 Composite for Electrochemical Sensing. *Talanta* **2007,** *71*, 1096-102.

(25) Pérez-López, B.; Merkoçi, A., Magnetic Nanoparticles Modified with Carbon Nanotubes for Electrocatalytic Magnetoswitchable Biosensing Applications. *Adv. Funct. Mater.* **2011,** *21*, 255-260.

(26) Zarei, H.; Ghourchian, H.; Eskandari, K.; Zeinali, M., Magnetic Nanocomposite of Anti-Human IgG/COOH-Multiwalled Carbon Nanotubes/Fe_3O_4 as a Platform for Electrochemical Immunoassay. *Anal. Biochem.* **2012,** *421*, 446-453.

(27) Hernández, J.; Thompson, I. M., Prostate□Specific Antigen: A Review of the Validation of the Most Commonly Used Cancer Biomarker. *Cancer* **2004,** *101*, 894-904.

(28) Fürstenberger, G.; Senn, H.-J., Insulin-Like Growth Factors and Cancer. *The lancet oncology* **2002,** *3*, 298-302.

(29) Engel, R. H.; Kaklamani, V. G., HER2-Positive Breast Cancer. *Drugs* **2007,** *67*, 1329-1341.

(30) Chen, B. J.; Wu, Y. L.; Tanaka, Y.; Zhang, W., Small Molecules Targeting c-Myc Oncogene: Promising Anti-Cancer Therapeutics. *Int. J. Biol. Sci.* **2014,** *10*, 1084-96.

(31) Dang, C. V., MYC on the Path to Cancer. *Cell* **2012,** *149*, 22-35.

(32) D J Liao; Dickson, R. B., c-Myc in Breast Cancer. *Endocr.-Relat. Cancer* **2000,** *7*, 143-164.

(33) Abdalla, A. M.; Ghosh, S.; Puri, I. K., Decorating Carbon Nanotubes with Co-Precipitated Magnetite Nanocrystals. *Diamond Relat. Mater.* **2016,** *66*, 90-97.

(34) Abdalla, A. M.; Fattah, A. R. A.; Ghosh, S.; Puri, I. K., Magnetoresponsive Conductive Colloidal Suspensions with Magnetized Carbon Nanotubes. *J. Magn. Magn. Mater.* **2017,** *421*, 292-299.

(35) Bean, C.; Livingston, J., Superparamagnetism. *J. Appl. Phys.* **1959,** *30*, S120-S129.

(36) Stefansson, S.; Kwon, H. H.; Ahn, S. N., Targeting Antibodies to Carbon Nanotube Field Effect Transistors by Pyrene Hydrazide Modification of Heavy Chain Carbohydrates. *J. Nanotechnol.* **2012,** *2012*, 1-8.

(37) Patolsky, F.; Weizmann, Y.; Willner, I., Long-Range Electrical Contacting of Redox Enzymes by SWCNT Connectors. *Angew. Chem., Int. Ed. Engl.* **2004,** *43*, 2113-2117.

(38) Zhang, X.; Wang, D.; Yang, D.; Li, S.; Shen, Z., Electronic Detection of Escherichia coli O157:H7 Using Single-Walled Carbon Nanotubes Field-Effect Transistor Biosensor. *Engineering* **2012,** *04*, 94-98.

(39) Salehi-Khojin, A.; Field, C. R.; Yeom, J.; Masel, R. I., Sensitivity of Nanotube Chemical Sensors at the Onset of Poole–Frenkel Conduction. *Appl. Phys. Lett.* **2010,** *96*, 163110.

(40) Salehi-Khojin, A.; Khalili-Araghi, F.; Kuroda, M.A.; Leburton, J.P.; Lin, K.Y.; Masel, R.I., On the Sensing Mechanism in Carbon Nanotube Chemiresistors. *ACS Nano* **2010,** *5*, 153-158.

(41) Yang, M.; Kostov, Y.; Rasooly, A., Carbon Nanotubes Based Optical Immunodetection of Staphylococcal Enterotoxin B (SEB) in Food. *Int. J. Food Microbiol.* **2008,** *127*, 78-83.

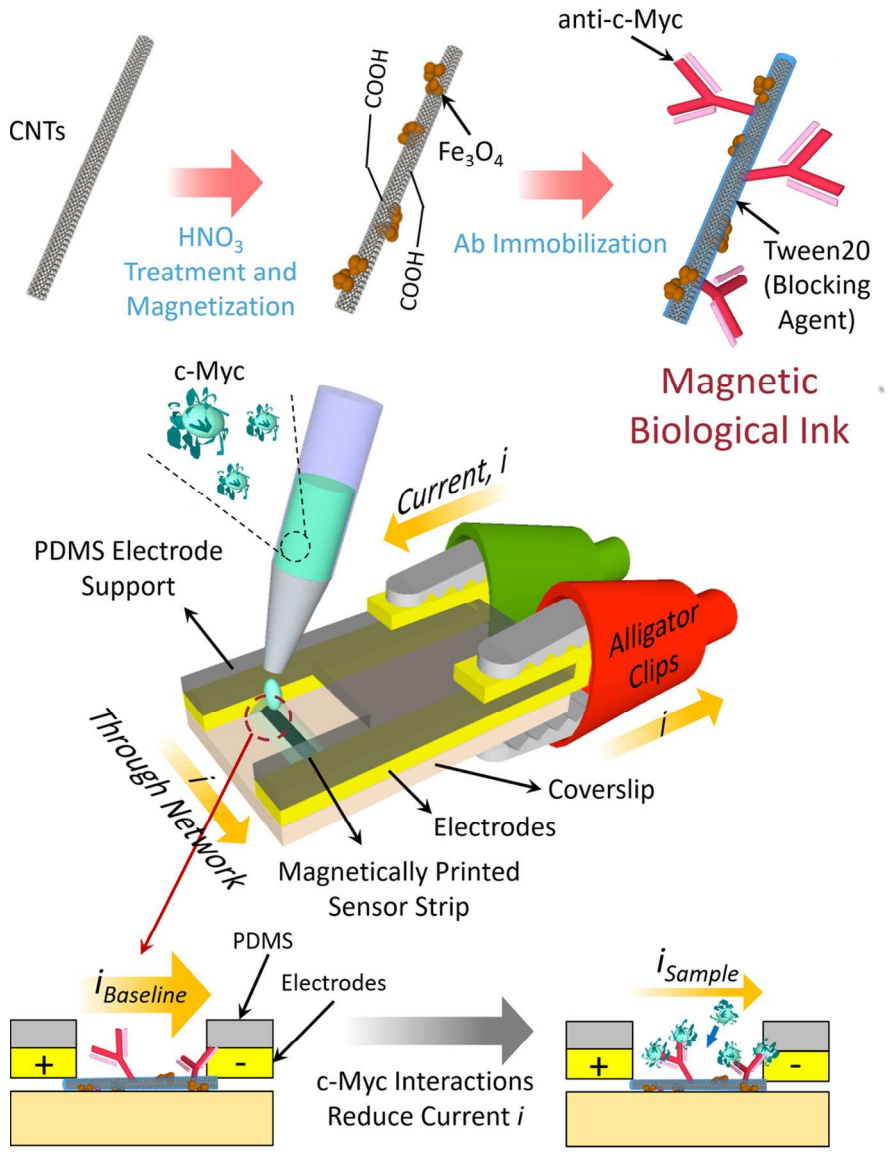

Figure 1. c-Myc Biosensor printing using a magnetic biological ink. Multiwalled CNTs are treated with concentrated nitric acid, which produces carboxylic (–COOH) active groups on the outer surfaces of the CNT. Some of these active groups act as nucleation sites for in situ co-precipitation of magnetite (Fe_3O_4) nanocrystals while the remainder remain available for forming covalent bonds with anti-c-Myc amine ($–NH_2$) groups. The CNT surfaces are blocked using Tween 20 to prevent non-specific interactions of Ag with the CNT surface. The magnetic biological ink is then deposited on a glass substrate using a pipette where it self organizes under the influence of an external magnetic field that guides the ink to print a dense electrically conducting strip. After the ink dispersant evaporates, the sensor strip is connected to an external circuit using electrodes. When an aqueous c-Myc solution is deposited on this strip, its electrical resistance increases. A programmable logic controller measures the current flowing through this patterned strip.

109x140mm (300 x 300 DPI)

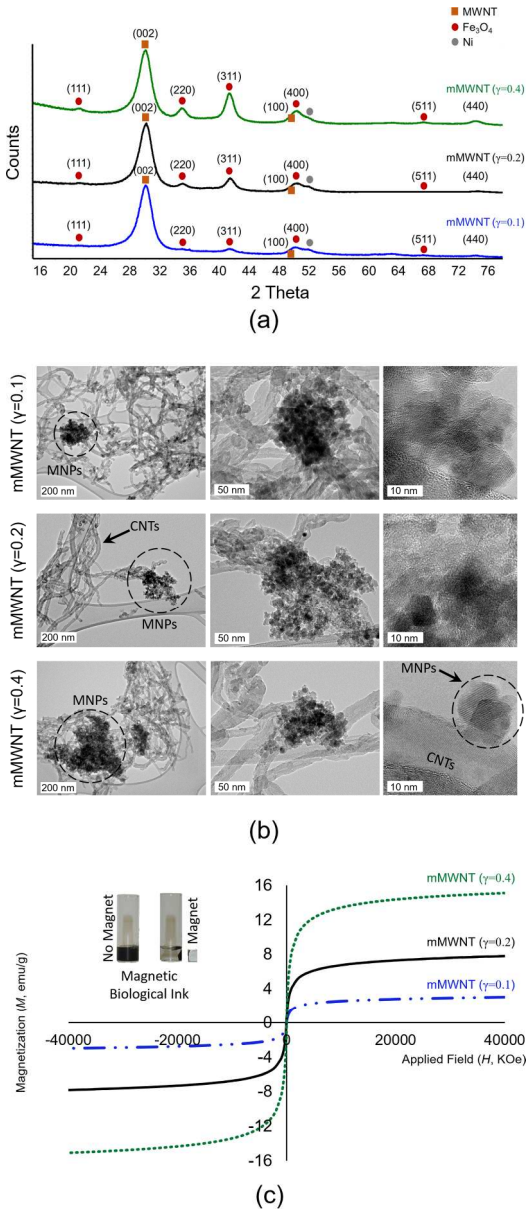

Figure 2. Characterization of Magnetized Multi-Walled Carbon Nanotubes. (a) X-Ray Diffraction Analysis of mCNTs. The XRD (Co K_α, λ=1.79 Å) patterns for magnetite to CNTs weight ratios γ = 0.1, 0.2, and 0.4 confirm the presence of a magnetite (Fe_3O_4) phase and a hexagonal carbon phase that originates from the carbon nanotubes. (b) TEM images of magnetized multiwall CNT samples at various magnetization weight ratios γ = 0.1 to 0.4 (from top to bottom) confirm that all samples have been successfully decorated with highly crystalline MNPs that are synthesized within a narrow size distribution around ~10 nm. (c) Magnetic Characterization. Magnetic hysteresis curves show that all magnetized CNT samples exhibit superparamagnetic behaviour, but have different saturation values Ms depending on γ. The greater the magnetite content, the stronger is the material response to a magnetic field.

196x453mm (300 x 300 DPI)

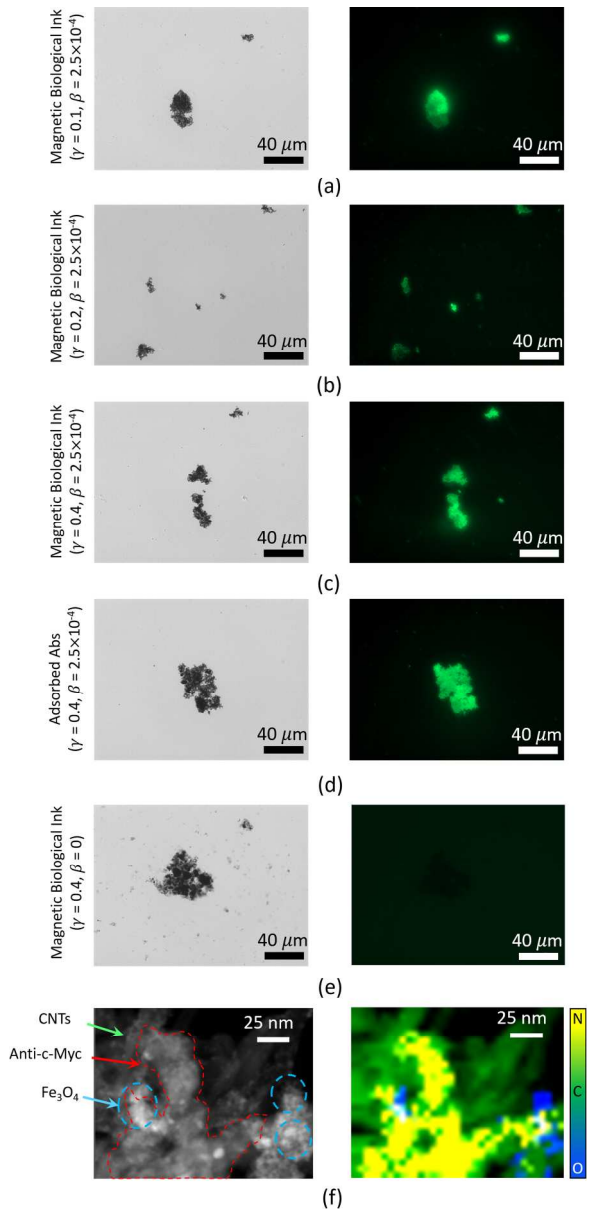

Figure 3. Visualization of Ab immobilization on the surface of magnetic CNTs. First, FITC- labeled fluorescent Abs are employed to confirm Ab immobilization on the surface of magnetic CNTs for an Ab:CNT weight ratio β = 2.5×10-4 in an ink where Abs are covalently bonded with magnetized CNTs that have Fe_3O_4:CNT weight ratios (a) γ = 0.1, (b) γ = 0.2 and (c) γ = 0.4, and (d) for an ink that contains Abs and MNPs, which are instead simply adsorbed on the surface of CNTs with γ = 0.4. For (e) β = 0, γ = 0.4, no fluorescence is observed from CNTs and Fe_3O_4, confirming that the fluorescence observed in (a)-(d) originates from FITC-labeled Abs only. No visual differences in fluorescence are detected for samples containing different weight ratios of magnetite, and those containing adsorbed and covalently bonded immobilized Abs and MNPs. For (a)-(e), the images on the left column are optical bright field and the images on the right column are bright field and fluorescent overlay. (f) STEM and EELS micrographs reveal the presence of elemental carbon (C), oxygen (O) and nitrogen (N). The nitrogen, which is present only in Anti-c-Myc Abs, confirms Ab immobilization on the conductive CNT network.

176x367mm (300 x 300 DPI)

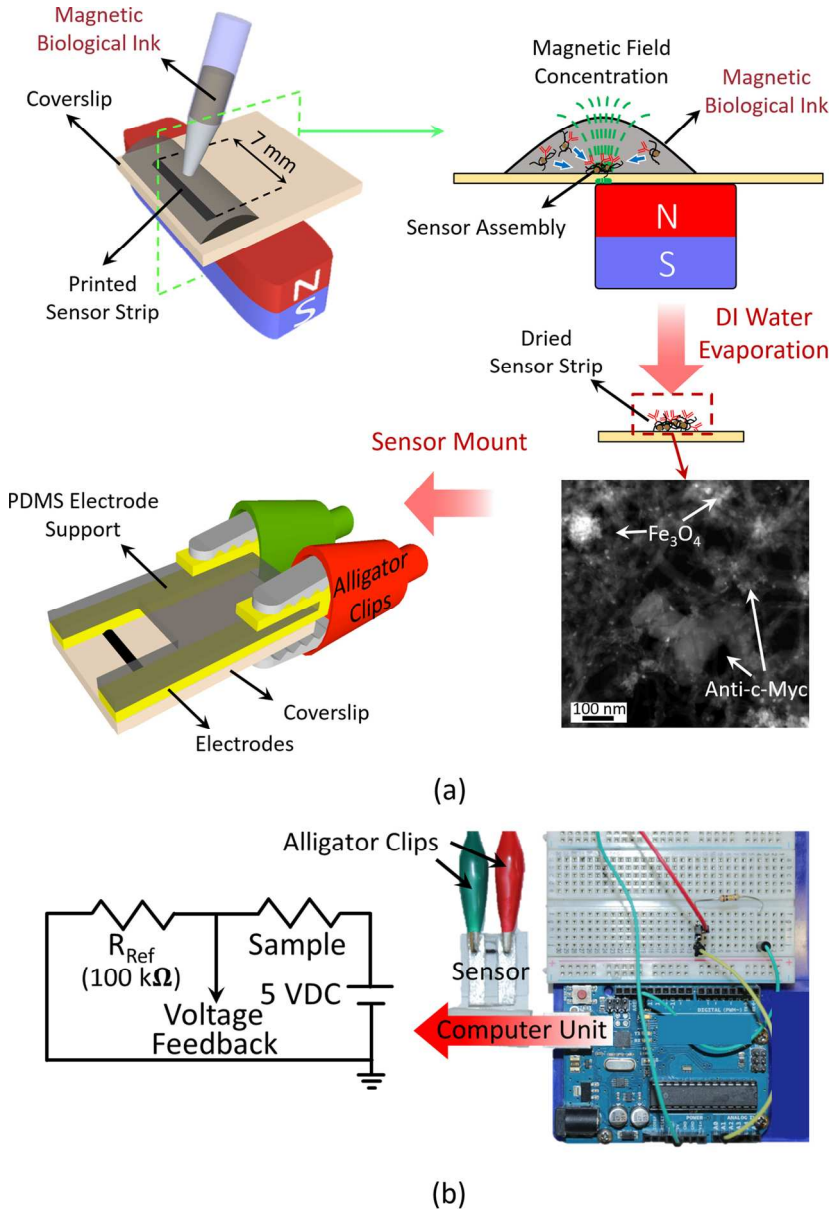

Figure 4. Printing technique and sensor assembly. (a) 10 µL of the magnetic bioink is deposited on top of a glass coverslip that is placed on a permanent magnet. The applied magnetic field concentrates and self organizes the functionalized magnetic CNTs on the substrate. After the supernatant in the ink is evaporated, a patterned strip of densely packed Ab-functionalized CNTs remains deposited on the substrate, which forms the sensor. The STEM micrograph identifies MNPs and anti-c-Myc that constitute the print based on the magnetic bioink. Electrodes are readily connected to either end of the strip, providing current to the sensor. (b) A voltage divider with a reference resistor R_{ref} = 100 kΩ monitors current changes that measure the biosensor responses to the various samples that are deposited on it.

124x182mm (300 x 300 DPI)

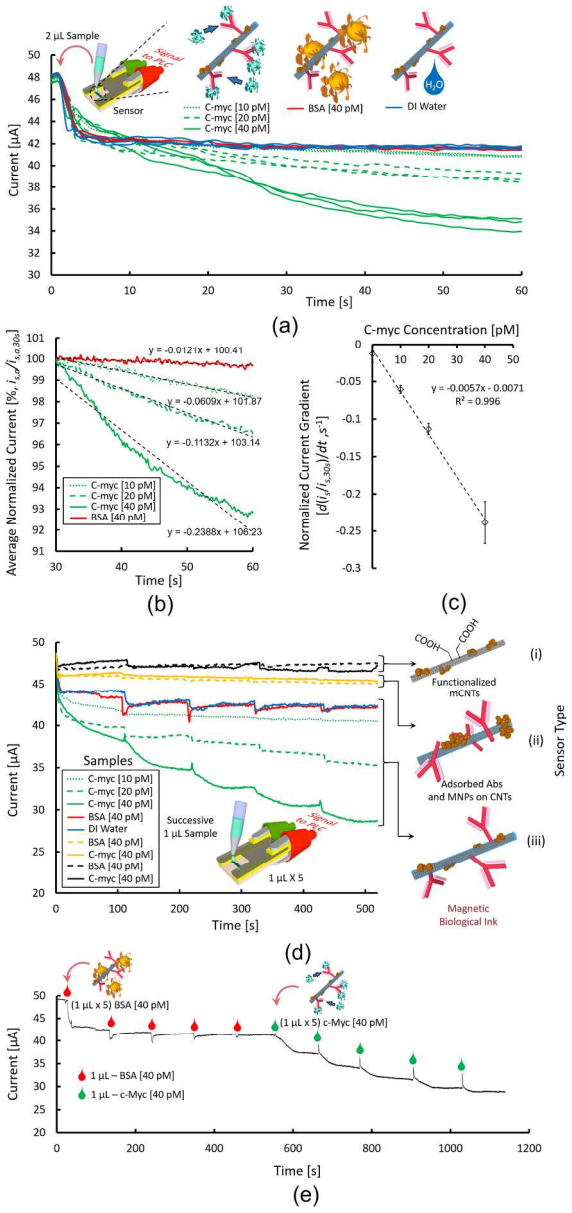

Figure 5. Biosensor transient response. (a) Immediately after 2 µL samples are deposited on the sensor strip, the DI water and BSA samples induce a rapid decrease in electrical current, whichsubsequently levels out. In contrast, since the sensor is inherently sensitive to c-Myc Ag interactions due to the anti-c-Myc Abs that are covalently bonded to the surfaces of CNTs, the current for all c-Myc samples decreases to levels below those measured for DI water and BSA deposition, which offers proof of targeted detection and sensor specificity to c-Myc Ags. The higher the c-Myc concentration in a sample, the larger the current decrease it induces. All of the deposited c-Myc samples produce a steady current decrease during the period 30 s < t < 60 s. Normalizing the average current over that duration leads to the quasi-linear response shown in (b). There is a linear correlation in (c) between the normalized current gradients in (b) and the corresponding c-Myc concentrations. **Biosensor response to successive 1 µL sample additions.** (d) Acting as a control, magnetized CNTs that are not functionalized with Abs (i) cannot distinguish between 40 pM BSA and c-Myc samples, black dashed and solid curves respectively. When anti-c-Myc is immobilized on the CNT surfaces through adsorption, again (ii) there is insufficient discrimination between these two samples. In contrast, a

sensor fabricated using an ink in which anti-cMyc is attached to the CNT surfaces through acid functionalization, (iii) clearly distinguishes between the two negative control samples, DI water and BSA, and the Ag of interest, c-Myc. (e) After the deposition of 5 successive 1 µL samples of BSA [40 pM], the biosensor response is relatively unchanged. Only after the introduction of c-Myc [40 pM] samples that the reduction in current is observed, validating the specificity of the sensor to the target antigen in the presence of another protein.

181x389mm (300 x 300 DPI)

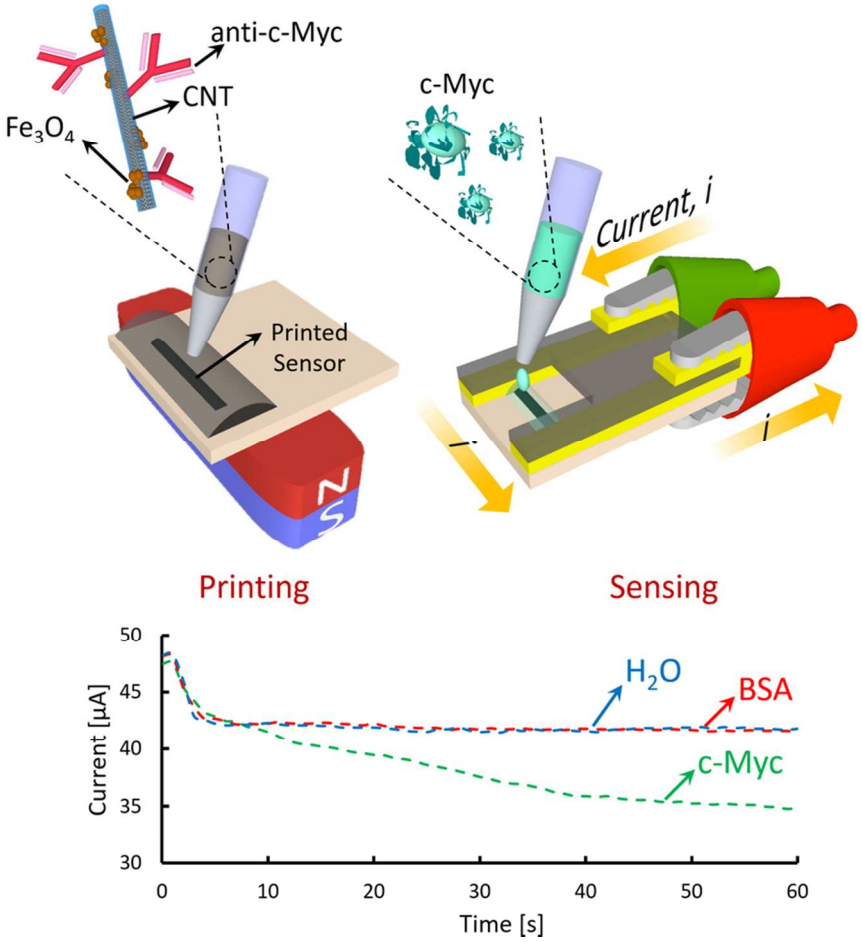

88x87mm (300 x 300 DPI)